Title

A {Ni12}-Wheel-Based Metal—Organic Framework for Coordinative Binding of Sulphur Dioxide and Nitrogen Dioxide

Journal

Angewandte Chemie International Edition, 61(6)

ISSN

1433-7851

Authors

Han, Zongsu

Li, Jiangnan

Lu, Wanpeng

et al.

Publication Date

2022-02-01

DOI

10.1002/anie.202115585

A $\{Ni_{12}\}$-wheel-based metal-organic framework for coordinative binding of sulphur dioxide and nitrogen dioxide

Zongsu Han[1§], Jiangnan Li[2§], Wanpeng Lu[2], Yinlin Chen[2], Xiaoping Zhang[1], Longfei Lin[3], Xue Han[2], Simon J. Teat[4], Mark D. Frogley[5], Sihai Yang*[2], Wei Shi*[1] and Peng Cheng[1]

[1] Key Laboratory of Advanced Energy Materials Chemistry (MOE), College of Chemistry, Nankai University, Tianjin 300071, China.

[2] Department of Chemistry, University of Manchester, Manchester M13 9PL, UK.

[3] Beijing National Laboratory for Molecular Science, Key Laboratory of Colloid and Interface and Thermodynamics Institute of Chemistry, Chinese Academy of Sciences, Beijing 100190, China.

[4] Advanced Light Source, Lawrence Berkeley National Laboratory, Berkeley CA 94720, USA.

[5] Diamond Light Source, Harwell Science Campus, Oxfordshire OX11 0DE, UK.

[§] These authors contributed equally to this work.

*Corresponding authors. E-mails: shiwei@nankai.edu.cn; Sihai.Yang@manchester.ac.uk

Abstract: Air pollutions by SO_2 and NO_2 have caused significant risks on the environment and human health. Understanding on the mechanism of active sites within capture materials is of fundamental importance for the development of new clean-up technologies. Here we report the crystallographic observation of reversible coordinative binding of SO_2 and NO_2 on open Ni(II) sites in a robust metal-organic framework (NKU-100) incorporating unprecedented $\{Ni_{12}\}$-wheels, which exhibit six open Ni(II) sites on each $\{Ni_{12}\}$-wheel. Immobilised gas molecules are further stabilised by cooperative host-guest interactions comprised of hydrogen bonds, π···π interactions and dipole interactions. At 298 K and 1.0 bar, NKU-100 shows adsorption uptakes of 6.21 and 5.80 mmol g^{-1} for SO_2 and NO_2, respectively. Dynamic breakthrough experiments have confirmed the selective retention of SO_2 and NO_2 at low concentrations under dry conditions. This work will inspire the future design of efficient sorbents for the capture of SO_2 and NO_2.

Keywords: metal-organic framework, SO_2 and NO_2 adsorptions, binding site, *in situ* synchrotron single crystal X-ray diffraction

INTRODUCTION

Metal-organic frameworks (MOFs) have emerged as multifunctional materials owing to their high internal surface area and capability of precise edition of pore functionality [1-3]. The fine tuning of pore size and geometry, framework topology, and chemical functionality has resulted in targeted applications, including gas adsorption, separation, catalysis, substrate binding and delivery, where host-guest interactions present and often dominate the materials function [4-10]. Thus, deriving deep understanding and placing control on

the mechanism of host-guest interactions are of critical importance for the design and discovery of new functional MOF materials. This is, however, a highly challenging task, not least because the supramolecular host-guest interactions often undergo dynamic process, where multiple binding sites of similar energies co-exist to induce the mobility and disorder of guest molecules in the pore [4,8]. MOFs bearing open metal sites (OMSs) can provide specific, localised binding of guest molecules, driving strong and highly selective adsorption of target gases [11-13].

Full retention of the crystallinity, ideally single crystallinity, of MOFs upon desolvation and binding of guest molecules is another major barrier in the study of host-guest interactions by advanced diffraction techniques. This barrier is pronounced in systems bearing isolated OMSs upon removal of coordinated solvent molecules and upon adsorption of highly reactive molecules, such as SO_2, NO_2 and NH_3, which can lead to irreversible coordination at the OMSs and thus influence framework stability. To date, MOF materials that can reversibly adsorb SO_2, NO_2 and NH_3 have only been reported in exceptional cases [4,8,13-17], where stable systems incorporating OMSs are extremely scarce [13].

Construction of MOFs using multinuclear metal clusters with high spatial connectivity can effectively enhance the density of OMSs within the framework and stability of the material [18,19]. However, such systems that can achieve reversible adsorption of SO_2 and NO_2 have not been reported to date. Here we describe the synthesis, crystal structure and gas adsorption and separation properties of a unique $\{Ni_{12}\}$-wheel-based MOF, $[NH_2(CH_3)_2]_6[Ni_{12}(L)_3(\mu_3\text{-}O)_6(HCOO)_6(H_2O)_6]$ (denoted as NKU-100; NKU = Nankai University; H_4L = biphenyl-3,3',5,5'-tetracarboxylic acid), which exhibits high isothermal uptake of SO_2 and NO_2 (6.21 and 5.80 mmol g^{-1}, respectively) at 298 K and 1.0 bar. Significantly, the full retention of the single crystal of NKU-100 on desolvation has enabled elucidation of the binding of SO_2 and NO_2 molecules on the active sites by *in situ* synchrotron single crystal X-ray diffraction (SCXRD) and synchrotron infrared (IR) single crystal microspectroscopy. These crystallographic and dynamic experiments established a detailed molecular mechanism consisting of the reversible coordination of SO_2 and NO_2 at the six open Ni(II) sites on the $\{Ni_{12}\}$-wheel (denoted as first coordination sphere in Fig. 1) and at oxygen centre and ligand sites (denoted as secondary coordination sphere in Fig. 1) at a crystallographic resolution.

RESULTS AND DISCUSSION

Synthesis and structure determination of NKU-100

Single crystals of NKU-100 were synthesised *via* the solvothermal reaction of $Ni(CH_3COO)_2{\cdot}4H_2O$ and H_4L in the mixture of dimethylformamide (DMF) and water at 170 ℃ for three days. Bulk NKU-100 can be synthesised by microwave reaction within 30 mins. Compared with the MOF, $[Ni_2(H_2O)_2(L)]$ [20], which is constructed by bridging one-dimensional (1D) $[NiO_4(OH_2)_2]_\infty$ chains by the same linker, the synthesis of NKU-100 requires a higher reaction temperature (170 vs 140 ℃) to afford the formation of the multi-nuclear $\{Ni_{12}\}$-wheels.

Single crystal diffraction of NKU-100, $[NH_2(CH_3)_2]_6[Ni_{12}(L)_3(\mu_3\text{-}O)_6(HCOO)_6(H_2O)_6]\cdot 12H_2O$, confirmed that it crystallised in trigonal *P*-3 space group with a 3D open framework structure (Table S1). There are two crystallographically independent nickel sites (Fig. 2a). Ni(1) is coordinated with six oxygen atoms from two ligands, two μ_3-O atoms, and two $HCOO^-$ ligand generated from the decomposition of DMF during the synthesis, and Ni(2) is also six-coordinated with oxygen atoms from two ligands, one water molecule, one μ_3-O atom, and two $HCOO^-$ groups. The alternative linkage of six Ni(1) and six Ni(2) atoms assembled an unprecedented $\{Ni_{12}\}$-wheel comprised of three layers. Six Ni(1) centres are linked by six μ_3-O atoms to form a $\{Ni_6O_6\}$ ring which is sandwiched by two $\{Ni_3(HCOO)_3\}$ triangles in a staggered configuration (Fig. 2b). The $\{Ni_3(HCOO)_3\}$ triangles and the $\{Ni_6O_6\}$ ring are connected by six μ_3-O atoms to form the $\{Ni_{12}\}$-wheel (Fig. 2c), which is further bridged to twenty neighbouring $\{Ni_{12}\}$-wheels by twelve ligands. This arrangement affords a 3D framework containing 1D triangle-shape channels running through *c* axis with the window size of 6.7 Å, after taking into account of the van der Waals radius of surface atoms (Fig. 2d). The channel is filled by free, disordered solvent molecules and dimethylammonium cations, which have been confirmed by ^1H nuclear magnetic resonance spectroscopy of digested samples (Fig. S1).

Considering the $\{Ni_{12}\}$-wheel and ligand as twelve-connected O_h-node and four-connected D_{4h}-node, respectively, the framework of NKU-100 can be simplified as 4,12-connected net with $(4\text{-c})^3(12\text{-c})$ stoichiometry. It is a 2-nodal ***shp*** topology with the short (Schläfli) vertex symbol of $\{4^{36};6^{30}\}\{4^4;6^2\}^3$ (Fig. 2e) [21]. Four types of twelve-core clusters have been reported in MOFs [22-31], and transition-metal-cluster-based MOFs are rarely observed (Fig. S2 and Table S2). NKU-100 represents an unprecedented member in this family.

The coordinated water molecule on Ni(2) can be readily removed upon heating at 420 K under dynamic vacuum for two hours to generate open Ni(II) site as confirmed by *in situ* SCXRD (see below). A small contraction of 1D triangle channel along the *ab* plane [from a=b=16.084(6) Å and c=12.091(7) Å to a=b=15.957(2) Å and c=12.100(2) Å] is observed in desolvated NKU-100, $[NH_2(CH_3)_2]_6[Ni_{12}(L)_3(\mu_3\text{-}O)_6(HCOO)_6]$ (Table S3). The loss of coordinated water has also been confirmed by thermogravimetric analysis coupled with mass spectrometry (TGA-MS) and *in situ* IR analysis (Figs. S3 and S4). TGA-MS confirmed the complete removal of both free solvents in the pore and coordinated water molecules on Ni(2) at 423 K. Variable temperature IR spectra show the complete disappearance of the band at 3529 cm^{-1} (assigned to the O-H stretching mode of water molecule) at 423 K. Powder X-ray diffraction (PXRD) analysis confirmed the bulk purity and excellent stability of NKU-100 in various organic solvents (Fig. S5) and aqueous solutions of pH 3-13 (Fig. S6), and upon heating to 523 K in air (Fig. S7).

Analysis of adsorption and separation of SO_2 and NO_2

N_2 adsorption isotherms at 77 K for desolvated NKU-100 show type-I profile with a Brunauer-Emmett-Teller (BET) surface area of 698 $m^2\ g^{-1}$ (Fig. S8a). Pore size distribution calculated by non-local density functional theory shows a peak centred at ~6.3 Å, which is in good agreement with that (6.7 Å) derived from

single crystal structure (Fig. S8b). Gas adsorption isotherms for CO_2 and SO_2 were recorded at 273-318 K (Figs. 3a, S9 and S10), and for NO_2 at 298 and 308 K (Fig. S11). The uptake of SO_2 at 273, 298, 308 and 318 K are 6.71, 6.21, 5.56 and 5.08 mmol g^{-1}, respectively, which are comparable with that of leading SO_2 sorbents (Table S4), such as Mg-MOF-74 (8.6 mmol g^{-1}) [32], SIFSIX-3-Ni (2.7 mmol g^{-1}) [33] and SIFSIX-2-Cu (6.5 mmol g^{-1}) [33], but lower than that (17.5 mmol g^{-1}) of MFM-170 [13] which has a much higher BET surface area of 2408 m^2 g^{-1}. The isothermal uptake of NO_2 at 298 K is 5.80 mmol g^{-1}, which is comparable with MFM-520 (4.5 mmol g^{-1}) [17] of similar porosity but is lower than MFM-300(Al) (14.1 mmol g^{-1}) [8], which has a higher BET surface area of 1370 m^2 g^{-1} (Table S5). NKU-100 shows an uptake of CO_2 of 3.67 mmol g^{-1} at 298 K, which is lower than MOF-74 materials (4.9 and 8.0 mmol g^{-1} for the Zn [34] and Mg [35] analogue, respectively) that bear a high density of OMSs (Table S6). The isosteric heats (Q_{st}) of adsorption for SO_2 and NO_2 in NKU-100 were calculated to be 71 and 74 kJ mol^{-1}, respectively, at the zero-surface coverage, which are notably higher than that (43 kJ mol^{-1}) of CO_2 (Figs. 3b and S12). Analysis of pure-component isotherms *via* ideal adsorbed solution theory (IAST) [36-39] affords adsorption selectivities for equimolar mixtures of SO_2/N_2, SO_2/CO_2, NO_2/N_2 and NO_2/CO_2 at 298 K and 1.0 bar (>5000, 220-940, >5000 and 21-23, respectively) (Fig. 3c). The very high IAST selectivity values (>5000) are subject to large uncertainties due to the extremely low uptake of N_2 and therefore should be used for qualitative comparisons only. PXRD analysis confirmed the retention of crystal structure of the sample after gas adsorption (Fig. S13). Cycling experiments of adsorption of SO_2 were conducted (Fig. 3d), which confirmed the retention of adsorption capacity over 25 cycles of adsorption and desorption in NKU-100.

To investigate the ability to capture SO_2 and NO_2 at low concentrations, dynamic breakthrough experiments were carried out with a fixed-bed packed with desolvated NKU-100 using a variety of SO_2/NO_2-containing (~2500 ppm) gas mixtures at 298 K and 1.0 bar (Fig. 4). NKU-100 exhibits highly selective retention of SO_2 and NO_2 at concentrations of ~2500 ppm, while N_2 can elute through the fixed-bed rapidly (Figs. 4a and 4b). The presence of CO_2 shows little effect on the retention of SO_2, but negative impact on the retention of NO_2, with retention time of 213 and 54 min g^{-1} for SO_2 and NO_2, respectively (Figs. 4c and S14). Interestingly, NKU-100 can separate the mixture of SO_2 and NO_2 with selective adsorption of the former without the reduction of adsorption capacity of SO_2; this is in sharp contrast the state-of-the-art MOF sorbents that all show selective retention of NO_2 in the presence of SO_2 (Fig. 4d) [8,17]. Thus, NKU-100 demonstrates the unusual selective binding of SO_2 over NO_2.

Determination of binding domains for adsorbed CO_2, SO_2 and NO_2. The binding domains of CO_2, SO_2 and NO_2 were studied by *in situ* synchrotron SCXRD. A single crystal of NKU-100 was activated by heating at 420 K under dynamic vacuum for four hours. The structural analysis of desolvated NKU-100 confirms the complete removal of free solvents in the pore and the coordinated water molecule on the Ni(2) site, generating six open Ni(II) sites on each $\{Ni_{12}\}$-wheel. Importantly, desolvated NKU-100 has shown full retention of the single crystallinity upon adsorption of SO_2 and NO_2. Refinement of the diffraction data for

the gas-dosed samples revealed significant residual electron densities, which were assigned to adsorbed SO_2, NO_2 and CO_2 molecules residing over three, three and two independent binding sites, to afford $[NH_2(CH_3)_2]_6[Ni_{12}(L)_3(\mu_3\text{-}O)_6(HCOO)_6(SO_2)_{4.2}]\cdot 2.7SO_2\cdot 1.8SO_2$, $[NH_2(CH_3)_2]_6[Ni_{12}(L)_3(\mu_3\text{-}O)_6(HCOO)_6(NO_2)_3]\cdot 3.6NO_2\cdot 2.4NO_2$, and $[NH_2(CH_3)_2]_6[Ni_{12}(L)_3(\mu_3\text{-}O)_6(HCOO)_6(CO_2)_3]\cdot 3.6CO_2$, respectively (Fig. 5 and Table S3).

In SO_2-loaded NKU-100 (Fig. 5a), SO_2(I) is bound to open Ni(2) site *via* its oxygen centre [Ni···OSO=2.09(2) Å]. SO_2(I) is further supplemented by a C-H···O=S hydrogen bond to the coordinated $HCOO^-$ ligand [OSO···C=3.11(3) Å; <C-H···O=122.1(1)°]. SO_2(II) is located inside the triangle channel and stabilised by a π···π interaction with the phenyl ring [centroid of SO_2···projection on the ring=3.83(1) Å]. SO_2(III) binds to the μ_3-O centre with an ultra-strong dipole interaction [O_2S···O=1.78(3) Å]. The binding dynamics of SO_2 within NKU-100 has also been investigated by *in situ* synchrotron IR micro-spectroscopy. With the increase of partial pressure of SO_2, the band at 3270 cm^{-1} (assigned to the C-H stretching mode of the $HCOO^-$ ligand) decreases in intensity [40], consistent with the formation of C-H···O=S hydrogen bonds with SO_2(I). Simultaneously, the intensities of bands at 2258, 2451 and 3434 cm^{-1} (assigned to the overtone bands of SO_2 [41,42]) increase with SO_2 partial pressure (Fig. S15). Compared with gaseous SO_2 [43], the vibration modes of adsorbed SO_2 molecules show large red-shifts of ~50 cm^{-1}, confirming the heavily confined dynamics of adsorbed SO_2 molecules within NKU-100.

Similarly, three binding sites were observed for adsorbed NO_2 molecules (Fig. 5b). NO_2(I) coordinates to Ni(2) [Ni···OSO=2.13(2) Å] and forms a C-H···O=N hydrogen bond with the coordinated $HCOO^-$ ligand [ONO···C=3.20(3) Å; <C-H···O=123.4(1)°]. NO_2(II) is also located inside the triangle channel and stabilised by a π···π interaction with the phenyl ring [centroid of NO_2···projection on the ring=3.80(1) Å]. Interestingly, NO_2(III) binds to the μ_3-O centre but with only a moderate dipole interaction [O_2N···O=2.26(4) Å]. This binding distance is much longer than that observed in SO_2-loaded NKU-100. This observation is in excellent agreement with the unusual selective binding of SO_2 in the breakthrough separation of SO_2/NO_2 mixture.

In contrast to the V-typed polar molecules of SO_2 and NO_2, CO_2 is a linear nonpolar molecule. Symmetric disposition of its polar bonds results in the coincidence of positive and negative centres and makes the binding of CO_2 unable at site III. Thus, only two binding sites of CO_2 were located (Fig. 5c). Nevertheless, CO_2(I) can be immobilised at Ni(2) with a distance of 2.10(2) Å and 3.17(2) Å to the carbon centre of $HCOO^-$ group with a C-H···O angle of 123.2(1)°. CO_2(II) is located inside the triangle channel and stabilised by a π···π interaction with the phenyl ring [centroid of CO_2···projection on the ring=3.75(12) Å].

Thus, the high uptakes of SO_2 and NO_2 of NKU-100 are promoted by the multiple host-guest interactions within both the first and second coordination spheres (Fig. 1). SO_2 and NO_2 molecules at site I are bound to the OMSs by the formation of coordination bonds in the first coordination sphere of NKU-100. In the second coordination sphere, supramolecular bonds comprised of π···π and dipole interactions dominate the binding between gas molecules and the MOF, generating site II and III in NKU-100. Tables S7-S9 give a comprehensive review of the host-guest interactions within MOF materials. Ni-MOF-74 is a benchmark

MOF bearing open Ni(II) sites, and CO_2 is bound at the Ni(II) site with a Ni-O distance of 2.08 Å [44], which is similar to NKU-100. $Ni_3(pzdc)_2(7\ Hade)_2$ [$pzdc^{3-}$ = 3,5-pyrazoledicarboxylate; Hade = adenine] can trap trace C_2H_2 by open Ni(II) sites with a Ni···C_2H_2 distance of 3.30 Å [45]. Significantly, NKU-100 represents the first example in porous materials showing reversible binding between open Ni(II) sites and SO_2/NO_2 molecules, and the full retention of the single crystal structure of NKU-100 upon regeneration from the *in situ* SCXRD experiment has been confirmed (Table S3).

CONCLUSION

The design of efficient MOFs to achieve the clean-up of SO_2 and NO_2 remains a challenging task for the development of clean air technologies. Understanding of the binding mechanism of active sites within the microenvironment of sorbent materials can afford fundamental insights into the design of new materials with desired selectivity. However, little success has been achieved for the adsorption of SO_2 and NO_2 in MOF materials due to their limited stability towards these corrosive gases defined by the intrinsically moderate coordination bonds between metal and ligand that constitute the MOF. We have described high adsorption of SO_2 and NO_2 (6.21 and 5.80 mmol g^{-1}, respectively, at 298 K and 1.0 bar) in a robust MOF, NKU-100, based upon an unprecedented {Ni_{12}}-wheel, which displays six individual open Ni(II) sites on desolvation. This resulted in a high surface density of 2.22 Ni(II) per 100 $Å^2$ on its interior. *In situ* synchrotron X-ray single crystal diffraction has revealed the reversible coordination of SO_2 and NO_2 at the Ni(II) sites and other "soft" binding sites within the second coordination sphere comprised primarily of the organic moieties. The host-guest binding dynamics has been investigated by *in situ* synchrotron IR microspectroscopy as a function of SO_2 loading. Dynamic breakthrough experiments have demonstrated the promising potential of NKU-100 in the selective capture of SO_2 and NO_2 at low concentrations from mixed gas streams.

SUPPLEMENTARY DATA

Supplementary data are available at NSR online. CCDC 2059776, 2059778-2059782 contain the supplementary crystallographic data for this paper. These data can be obtained free of charge from the Cambridge Crystallographic Data Centre *via* www.ccdc.cam.ac.uk/data_request/cif. Correspondence and requests for materials should be addressed to W.S. and S.Y.

FUNDING

This work was supported by the National Natural Science Foundation of China (grant numbers 21622105, 21931004 and 21861130354), the Natural Science Foundation of Tianjin (grant number 18JCJQJC47200), the Ministry of Education of China (grant number B12015), the University of Manchester and the Royal Society. S.Y. and W.S. acknowledge the receipt of a Royal Society Newton Advanced Fellowship (NAF\R1\180297). We thank Diamond Light Source for access to Beamline B22. This research used resources of

Beamline 12.2.1 at the Advanced Light Source, which is a DOE Office of Science User Facility under contract no. DE-AC02-05CH11231.

AUTHOR CONTRIBUTIONS

Z.H.: synthesis and characterisation of NKU-100. J.L., W.L., Y.C. and X.H.: collection and analysis of gas adsorption and breakthrough data. W.L., L.L. and M.D.F.: measurements and analysis of synchrotron FTIR data. X.Z.: study of original structure of NKU-100. Z.H., J.L., S.J.T. and S.Y.: collection and analysis of synchrotron X-ray diffraction data. S.Y. and W.S.: design of the experiments. Z.H., S.Y., W.S. and P.C.: preparation of the manuscript with contribution from all authors.

Conflict of interest statement. None declared.

REFERENCES

1. Zhou HC, Long JR and Yaghi OM. Introduction to metal-organic frameworks. *Chem Rev* 2012; **112**: 673-2.

2. Batten SR, Champness NR and Chen XM *et al*. Terminology of metal-organic frameworks and coordination polymers (IUPAC Recommendations 2013). *Pure Appl Chem* 2013; **85**: 1715-10.

3. Dincă M and Long JR. Introduction: porous framework chemistry. *Chem Rev* 2020; **120**: 8037-2.

4. Yang S, Sun J and Ramirez-Cuesta AJ *et al*. Selectivity and direct visualization of carbon dioxide and sulfur dioxide in a decorated porous host. *Nat Chem* 2012; **4**: 887-8.

5. Chaemchuen S, Kabir NA and Zhou K *et al*. Metal-organic frameworks for upgrading biogas via CO_2 adsorption to biogas green energy. *Chem Soc Rev* 2013; **42**: 9304-29.

6. Nugent P, Belmabkhout Y and Burd SD *et al*. Porous materials with optimal adsorption thermodynamics and kinetics for CO_2 separation. *Nature* 2013; **495**: 80-5.

7. Barea E, Montoro C and Navarro JAR. Toxic gas removal-metal-organic frameworks for the capture and degradation of toxic gases and vapours. *Chem Soc Rev* 2014; **43**: 5419-12.

8. Han X, Godfrey HGW and Briggs L *et al*. Reversible adsorption of nitrogen dioxide within a robust porous metal-organic framework. *Nat Mater* 2018; **17**: 691-6.

9. Ding M, Flaig RW and Jiang HL *et al*. Carbon capture and conversion using metal-organic frameworks and MOF-based materials. *Chem Soc Rev* 2019; **48**: 2783-6.

10. Tchalala MR, Bhatt PM and Chappanda KN *et al*. Fluorinated MOF platform for selective removal and sensing of SO_2 from flue gas and air. *Nat Commun* 2019; **10**: 1328-10.

11. Dincă M, Dailly A and Liu Y *et al*. Hydrogen storage in a microporous metal-organic framework with exposed Mn^{2+} coordination sites. *J Am Chem Soc* 2006; **128**: 16876-8.

12. Sato H, Kosaka W and Matsuda R *et al*. Self-accelerating CO sorption in a soft nanoporous crystal. *Science* 2014; **343**: 167-4.

13. Smith GL, Eyley JE and Han X *et al*. Reversible coordinative binding and separation of sulfur dioxide in a robust metal-organic framework with open copper sites. *Nat Mater* 2019; **18**: 1358-8.

14. Savage M, Cheng Y and Easun TL *et al*. Selective adsorption of sulfur dioxide in a robust metal-organic framework material. *Adv Mater* 2016; **28**: 8705-7.

15. Carter JH, Han X and Moreau FY *et al*. Exceptional adsorption and binding of sulfur dioxide in a robust zirconium-based metal-organic framework. *J Am Chem Soc* 2018; **140**: 15564-4.

16. Li L, Silva I and Kolokolov DI *et al*. Post-synthetic modulation of the charge distribution in a metal-organic framework for optimal binding of carbon dioxide and sulfur dioxide. *Chem Sci* 2019; **10**: 1472-11.

17. Li J, Han X and Zhang X *et al*. Capture of nitrogen dioxide and conversion to nitric acid in a porous metal-organic framework. *Nat Chem* 2019; **11**: 1085-6.

18. Li YW, Li JR and Wang LF *et al*. Microporous meta-organic frameworks with open metal sites as sorbents for selective gas adsorption and fluorescence sensors for metal ions. *J Mater Chem A* 2013; **1**: 495-5.

19. Chen Z, Hanna SL and Redfern LR *et al*. Reticular chemistry in the rational synthesis of functional zirconium cluster-based MOFs. *Coord Chem Rev* 2019; **386**: 32-18.

20. Zhang X, Chen W and Shi W *et al*. Highly selective sorption of CO_2 and N_2O and strong gas-framework interactions in a nickel(II) organic material. *J Mater Chem A* 2016; **4**: 16198-7.

21. Feng D, Gu ZY and Chen YP *et al*. A highly stable porphyrinic zirconium metal-organic framework with shp-a topology. *J Am Chem Soc* 2014; **136**: 17714-4.

22. Sumida K, Hill MR and Horike S *et al*. Synthesis and hydrogen storage properties of $Be_{12}(OH)_{12}$(1,3,5-benzenetribenzoate)$_4$. *J Am Chem Soc* 2009; **131**: 15120-2.

23. Reinsch H, Feyand M and Ahnfeldt T *et al*. CAU-3: A new family of porous MOFs with a novel Al-based brick: $[Al_2(OCH_3)_4(O_2C\text{-}X\text{-}CO_2)]$(X=aryl). *Dalton Trans* 2012; **41**: 4164-8.

24. Li Z, Ye Y and Yao Z *et al*. An antiferromagnetic metalloring pyrazolate (Pz) framework with $[Cu_{12}(\mu_2\text{-}OH)_{12}(Pz)_{12}]$ nodes for separation of C_2H_2/CH_4 mixture. *J Mater Chem A* 2018; **6**: 19681-8.

25. Lysova AA, Samsonenko DG and Dorovatovskii PV *et al*. Tuning the molecular and cationic affinity in a series of multifunctional metal-organic frameworks based on dodecanuclear Zn(II) carboxylate wheels. *J Am Chem Soc* 2019; **141**: 17260-10.

26. Lysova AA, Samsonenko DG and Kovalenko KA *et al*. A series of mesoporous metal-organic frameworks with tunable windows sizes and exceptionally high ethane over ethylene adsorption selectivity. *Angew Chem Int Ed* 2020; **59**: 20561-7.

27. Cliffe MJ, Castillo-Martínez E and Wu Y *et al*. Metal-organic nanosheets formed *via* defect-mediated transformation of a hafnium metal-organic framework. *J Am Chem Soc* 2017; **139**: 5397-8.

28. Ji P, Manna K and Lin Z *et al*. Single-site cobalt catalysts at new $Zr_{12}(\mu_3\text{-}O)_8(\mu_3\text{-}OH)_8(\mu_2\text{-}OH)_6$ metal-organic framework nodes for highly active hydrogenation of nitroarenes, nitriles, and isocyanides. *J Am Chem Soc* 2017; **139**: 7004-8.

29. Cao L, Lin Z and Shi W *et al*. Exciton migration and amplified quenching on two-dimensional metal-organic layers. *J Am Chem Soc* 2017; **139**: 7020-10.

30. Zhang R, Meng DX and Ge FY *et al*. Tetrazole-based porous metal-organic frameworks for selective CO_2 adsorption and isomerization studies. *Dalton Trans* 2020; **49**: 2145-6.

31. Wang S, Kitao T and Guillou N *et al*. A phase transformable ultrastable titanium-carboxylate framework for photoconduction. *Nat Commun* 2018; **9**: 1660-9.

32. Tan K, Canepa P and Gong Q *et al*. Mechanism of preferential adsorption of SO_2 into two microporous paddle wheel frameworks $M(bdc)(ted)_{0.5}$. *Chem Mater* 2013; **25**: 4653-10.

33. Cui X, Yang Q and Yang L *et al*. Ultrahigh and selective SO_2 uptake in inorganic anion-pillared hybrid porous materials. *Adv Mater* 2017; **29**: 1606929-9.

34. Millward AR and Yaghi OM. Metal-organic frameworks with exceptionally high capacity for storage of carbon dioxide at room temperature. *J Am Chem Soc* 2005; **127**: 17998-2.

35. Zhai QG, Bu X and Mao C *et al*. Systematic and dramatic tuning on gas sorption performance in heterometallic metal-organic frameworks. *J Am Chem Soc* 2016; **138**: 2524-4.

36. Myers AL and Prausnitz JM. Thermodynamics of mixed-gas adsorption. *AIChE J* 1965; **11**: 121-7.

37. Heuchel M, Snurr RQ and Buss E. Adsorption of CH_4-CF_4 mixtures in silicalite: simulation, experiment, and theory. *Langmuir* 1997; **13**: 6795-10.

38. Bae YS, Mulfort KL and Frost H *et al*. Separation of CO_2 from CH_4 using mixed-ligand metal-organic frameworks. *Langmuir* 2008; **24**: 8592-7.

39. Zhang X, Xu N and Zhang SY *et al*. From 1D zigzag chains to 3D chiral frameworks: synthesis and properties of praseodymium (III) and neodymium (III) coordination polymers. *RSC Adv* 2014; **4**: 40643-8.

40. Wilmshurst JK. A vibrational assignment for methyl formate and methyl acetate. *J Mol Spectrosc* 1957; **1**: 201-15.

41. Samadhi TW, Jones LE and Clare AG. Influence of carbon on SO_X emissions from glass processing. *J Am Ceram Soc* 2003; **86**: 2044-6.

42. Watson IA, Henry BR and Ross IG. Local mode behavior: The Morse oscillator model. *Spectrochim Acta* 1981; **37**: 857-9.

43. Yang S, Liu L and Sun J *et al*. Irreversible network transformation in a dynamic porous host catalyzed by sulfur dioxide. *J Am Chem Soc* 2013; **135**: 4954-4.

44. Kim H, Sohail M and Yim K *et al*. Effective CO_2 and CO separation using [M_2(DOBDC)] (M = Mg, Co, Ni) with unsaturated metal sites and excavation of their adsorption sites. *ACS Appl Mater Interfaces* 2019; **11**: 7014-8.

45. Zhang Z, Peh SB and Wang Y *et al*. Efficient trapping of trace acetylene from ethylene in an ultramicroporous metal-organic framework: synergistic effect of high-density open metal and electronegative sites. *Angew Chem Int Ed* 2020; **59**: 18927-6.

Figures and legends

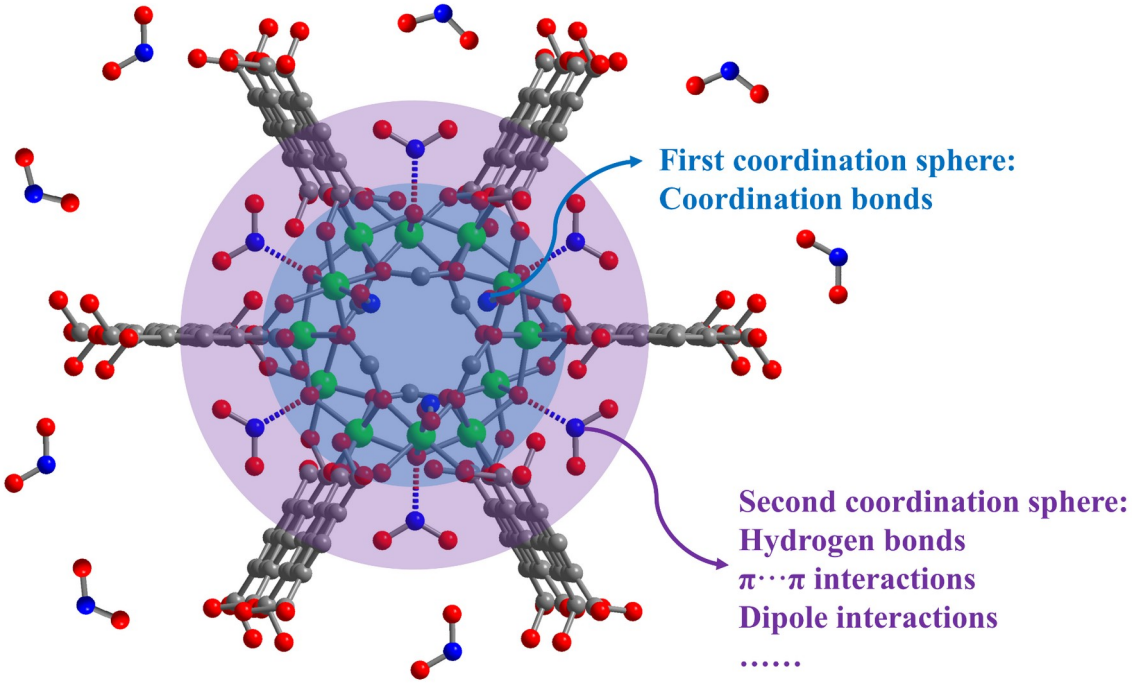

Fig. 1. Illustration of host-guest interactions within first (blue) and second (purple) coordination spheres of the $\{Ni_{12}\}$-wheel in NKU-100.

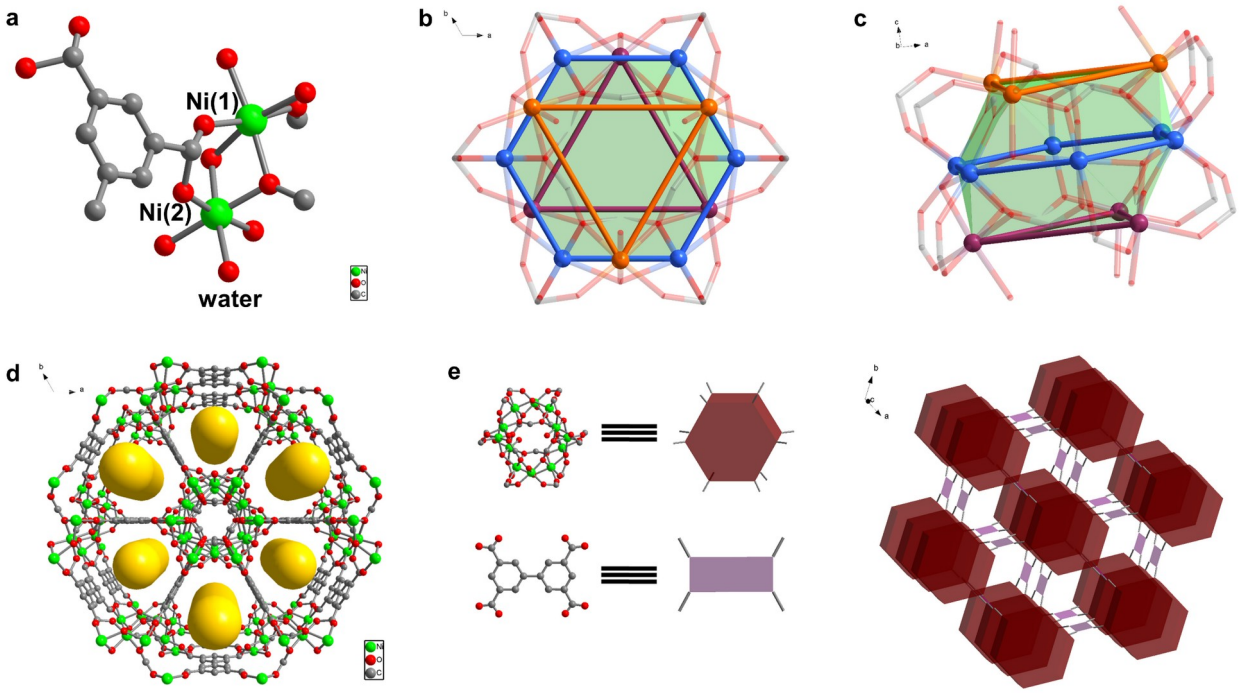

Fig. 2. Single crystal structure of NKU-100. **a.** Minimum structural unit. **b.** Vertical view of the $\{Ni_{12}\}$-wheel of NKU-100. **c.** Lateral view of the wheel of NKU-100. **d.** Framework structure and triangle channel along *c* axis. **e.** Topology of NKU-100.

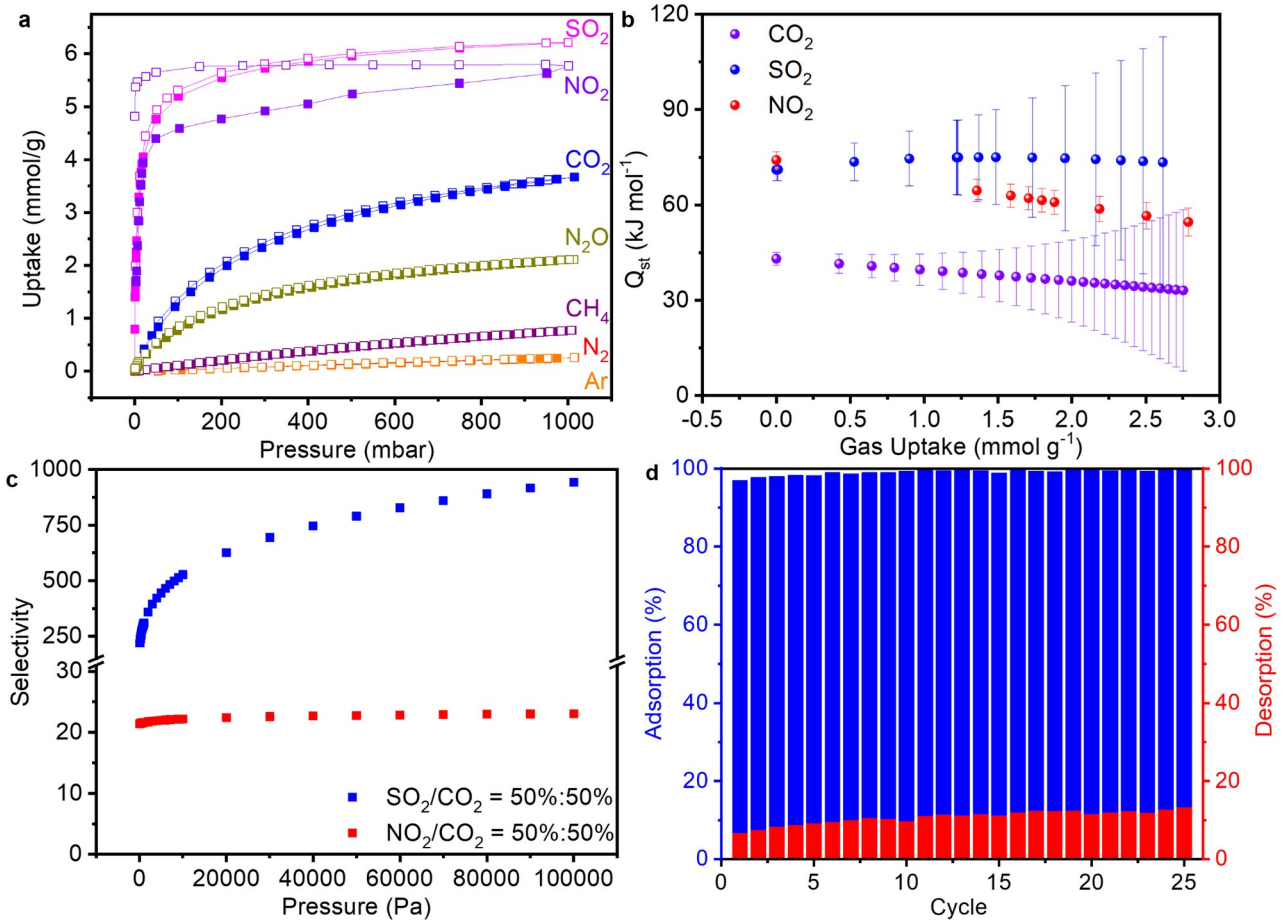

Fig. 3. Gases adsorptions of NKU-100. (a) Gases adsorption isotherms for different gases of NKU-100 at 298 K. (b) *Q*st for NKU-100 with CO_2/SO_2/NO_2. (c) IAST selectivities for CO_2/SO_2 (50% CO_2 and 50% SO_2) and CO_2/NO_2 (50% CO_2 and 50% NO_2) at 298 K. (d) Recycling experiments for NKU-100 for SO_2 at 298 K.

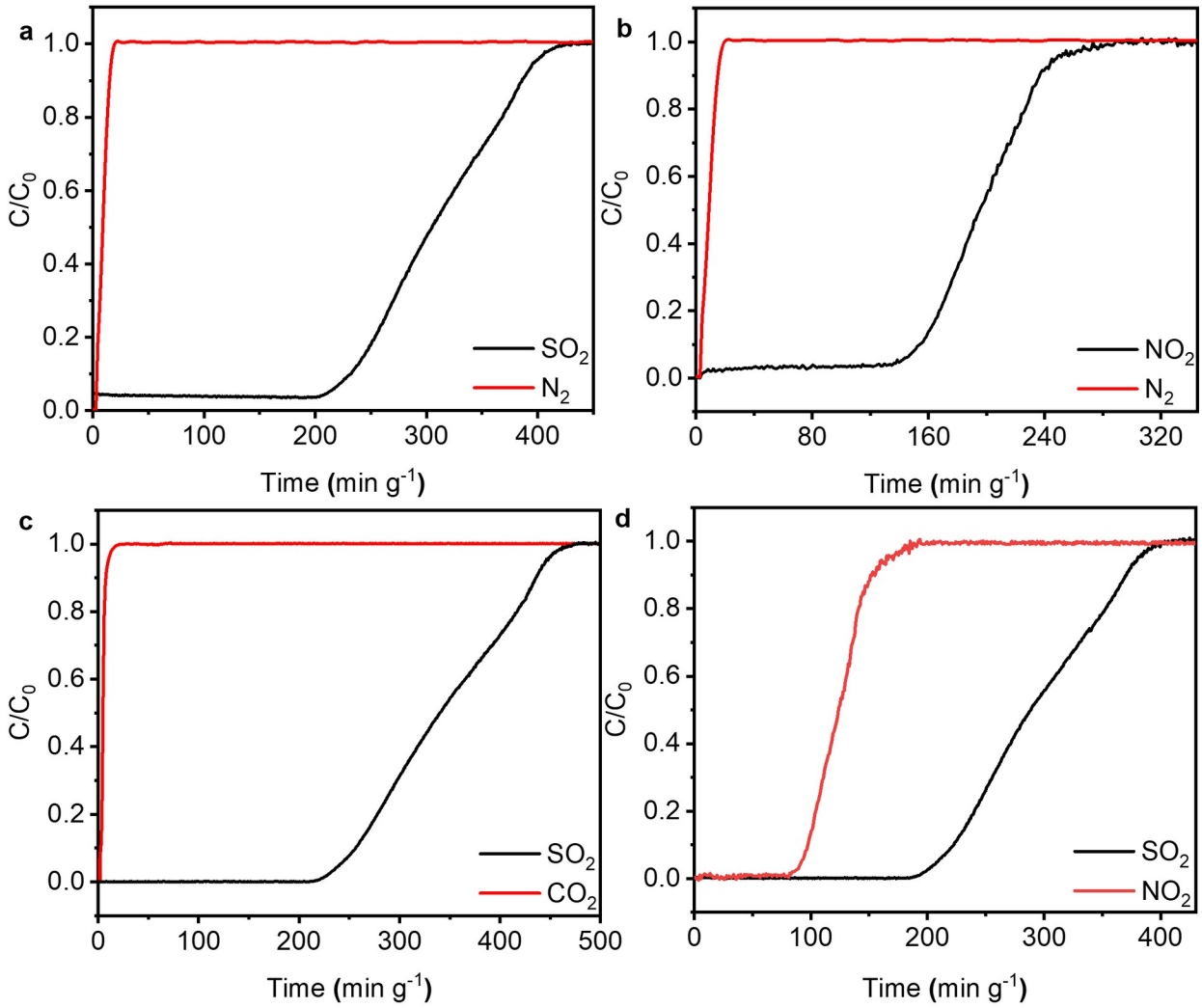

Fig. 4. Breakthrough experiments for NKU-100 at (a) N_2/SO_2 (0.25% SO_2 and 50% N_2 diluted in He), (b) N_2/NO_2 (0.25% NO_2 and 50% N_2 diluted in He), (c) SO_2/CO_2 (0.42% SO_2 and 15% CO_2 diluted in He), (d) NO_2/SO_2 (0.25% NO_2 and 0.25% SO_2 diluted in He).

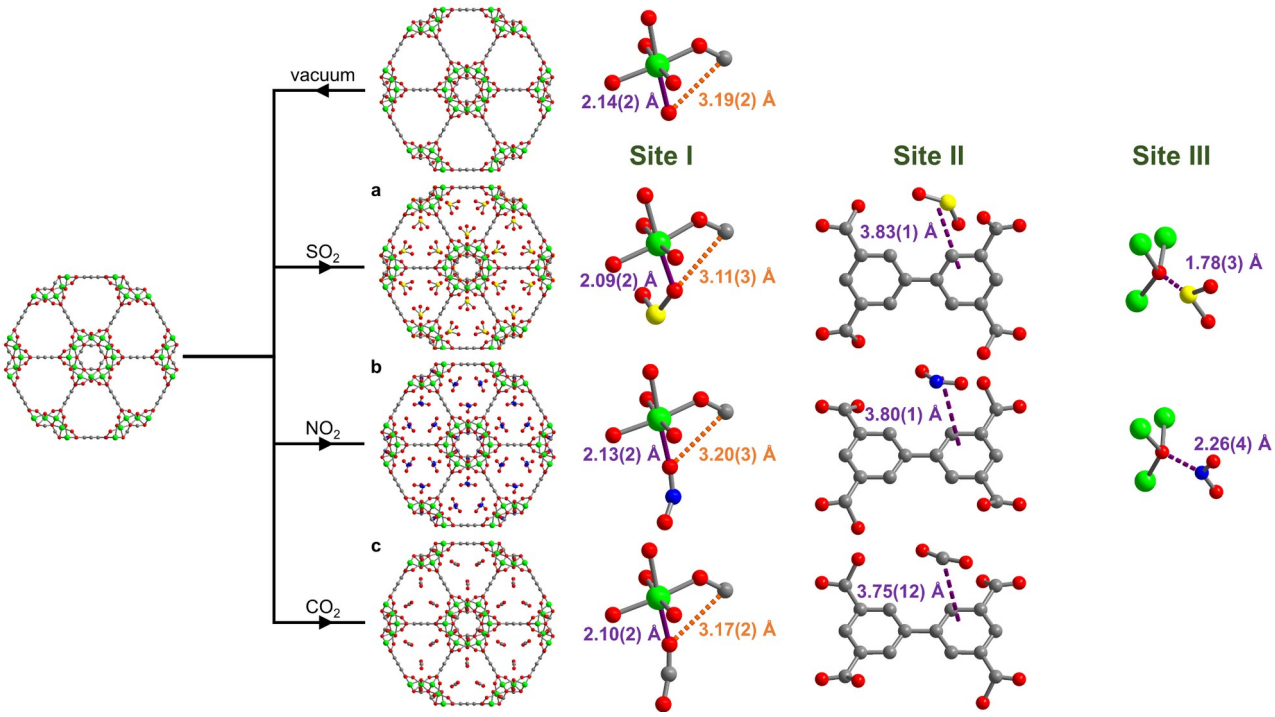

Fig. 5. *In situ* synchrotron SCXRD analysis. From left to right: activated NKU-100, original NKU-100 and (a) NKU-100-SO_2, (b) NKU-100-NO_2, (c) NKU-100-CO_2 along *c* axis. There are two binding sites of NKU-100 in CO_2 and three in SO_2/NO_2. Green ball represents Ni, blue for N, grey for C, red for O and yellow for S.

TOC:

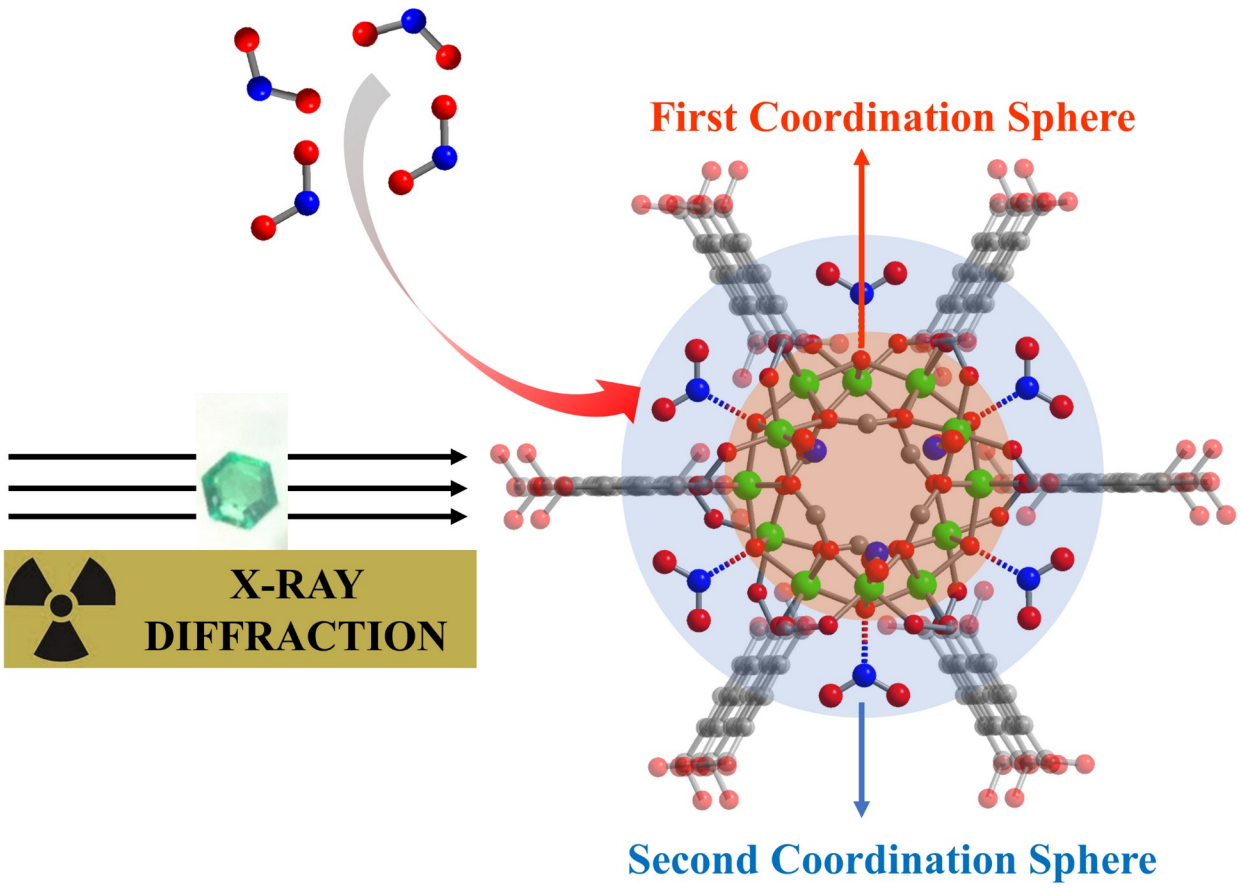
First Coordination Sphere
X-RAY
DIFFRACTION
Second Coordination Sphere